COMMUNICATION

Monolayer hydrophilic MoS_2 with strong charge trapping for atomically thin neuromorphic vision systems

Received 00th January 20xx,
Accepted 00th January 20xx

DOI: 10.1039/x0xx00000x

Yunxia Hu, [ab] Mingjin Dai, [ab] Wei Feng, [c] Xin Zhang, [b] Shichao Zhang, [b] Biying Tan, [b] Huiming Shang, [b] YongQing Fu,[d] PingAn Hu[*ab]

Effective control of electrical and optoelectronic properties of two-dimensional layered materials, one of the key requirements for applications in advanced optoelectronics with multiple functions, has been hindered by the difficulty of elemental doping, which is commonly utilized in Si technology. In this study, we proposed a new method to synthesize hydrophilic MoS_2 monolayers through covalently introducing hydroxyl groups during their growth process. These hydroxyl groups exhibit a strong capability of charge trapping, and thus the hydrophilic MoS_2 monolayers achieve excellent electrical, optical, and memory properties. Optical memory transistors, made from a single component of monolayer hydrophilic MoS_2, exhibit not only excellent light-dependent and time-dependent photoelectric performance, but also good photo-responsive memory characteristics with multi-bit storage and more than 10^4 switching ratios. Atomically thin neuromorphic vision systems (with a concept of proof of 10×10 neuromorphic visual image) are manufactured from arrays of hydrophilic MoS_2 optical memory transistors, showing high quality image sensing and memory functions with a high color resolution. These results proved our new concepts to realize image memorization and simplify the pixel matrix preparation process, which is a significant step toward the development of future artificial visual systems.

New concepts

Due to the ability to simulate the functions of biological vision systems, neuromorphic visual sensors are expected to simplify the integration of photodetectors, memory devices and processing units in artificial visual systems and reduce power consumption. However, it is difficult to apply existing materials in the high-density device integration due to the challenge in further scaling down the size of sensors and the lack of large-size atomically thin materials. Here we report a monolayer hydrophilic MoS_2 film by covalently introducing hydroxyl groups with strong charge trapping, which can makes the realization of neuromorphic vision systems. The monolayer hydrophilic MoS_2 optical memory transistors have photo-responsive memory characteristics with multi-bit storage and more than 10^4 switching ratio. The corresponding atomically thin neuromorphic vision systems exhibit excellent capabilities of image sensing, image memorization, and color discrimination. It is believed that our results provide a significant pathway towords the material science and neuromorphic visual systems.

Introduction

Two-dimensional (2D) semiconductor materials have been considered as good candidates for next generation electronic and optoelectronic devices due to their unique and unprecedented electrical, optical and mechanical properties compared to those of bulk materials.[1-7] To date, 2D semiconductor materials have shown significant prospects in many applications, such as photodetectors, [8,9] field-effect transistors,[7,10,11] flexible sensors[12] and optoelectronic memories[13,14]. As a representative 2D semiconductor material, molybdenum disulfide (MoS_2) can be transformed from an indirect band gap material to a direct band gap one as the thickness is decreased to a single layer. This is accompanied by a significant enhancement of its photoluminescence (PL) efficiency, making it promising among many advanced functional materials for sensing, biology and optoelectronics applications.[4,15] However, it is often difficult to rationally modulate optical, electrical and memory properties of these 2D semiconductor materials using the conventional process (such as element doping, commonly used in silicon technology) because of their intrinsic structural stability. This severely limits their successful applications for advanced electronic devices required for multiple functions, such as those in neuromorphic vision systems.

Artificial visual system, inspired by the human visual

[a.] *School of Materials Science and Engineering, Harbin Institute of Technology, Harbin 150001, P. R. China. E-mail: hupa@hit.edu.cn.*
[b.] *MOE Key Laboratory of Micro-Systems and Micro-Structures Manufacturing, Harbin Institute of Technology, Harbin 150001, P. R. China.*
[c.] *College of Chemistry, Chemical Engineering and Resource Utilization, Northeast Forestry University, Harbin 150040, P. R. China.*
[d.] *Faculty of Engineering & Environment, Northumbria University, Newcastle upon Tyne, NE1 8ST, UK.*
†Electronic Supplementary Information (ESI) available:See DOI: 10.1039/x0xx00000x

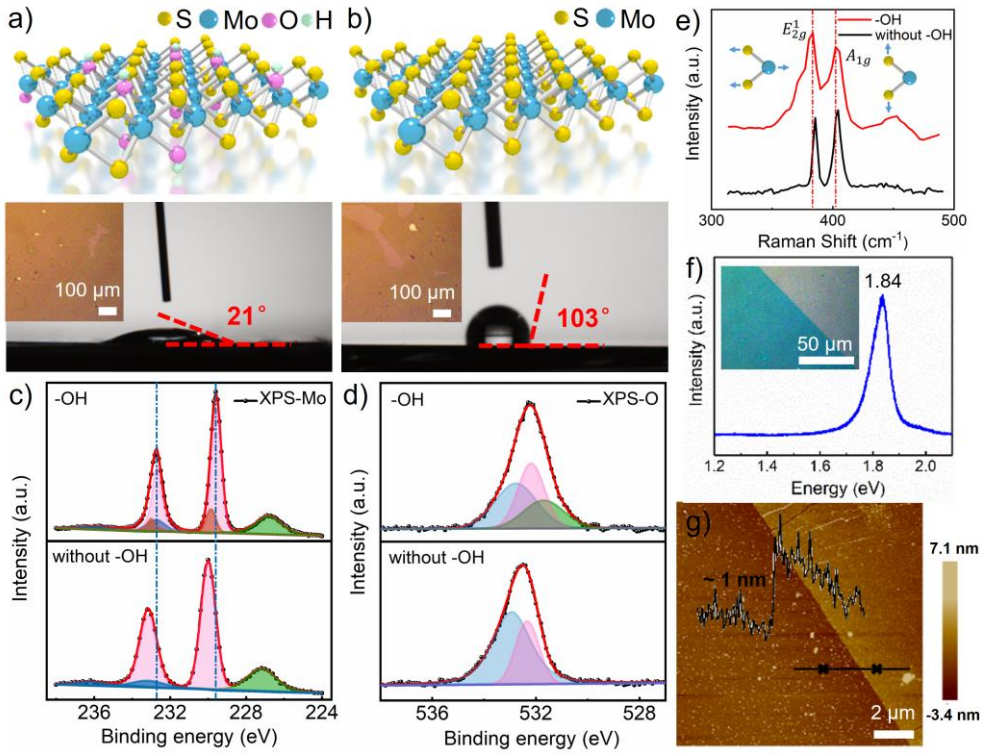

Fig. 1 Characterization of monolayer hydrophilic MoS_2. (a) Schematic diagram and the contact angle of MoS_2 with −OH. (b) Schematic diagram and the contact angle of MoS_2 without −OH. (c) XPS spectra of Mo peak for MoS_2 samples synthesized with KOH and without KOH. (d) XPS spectra of O peak for MoS_2 samples synthesized with KOH and without KOH. (e) Raman spectra of the MoS_2 with −OH and without –OH on SiO_2 substrates. (f) PL spectrum of the monolayer hydrophilic MoS_2 on the SiO_2 substrate. (g) The AFM topography image of an isolated monolayer MoS_2 and the corresponding height profile extracted from the white line (inset).

system to create recognition and memorization of various visual information such as objects and colors in a complex environment, has recently attracted significant research attention.[16-24] Conventional neuromorphic visual systems are consisted of photodetectors, memory devices and processing units. They can convert optical signals into electrical ones, store digital images and conduct complex image recognition, exhibiting great application prospects in the fields of artificial intelligence, humanoid robotics and visual prostheses. [16-18] Considering the requirements of neuromorphic visual systems in terms of miniaturization capabilities, which are the key capabilities enabling the production of modern integrated circuitry, 2D semiconductor materials are one of the best choices for system miniaturization/integration in image sensor circuitry.[13,25-28] Additionally, artificial vision system requires that its device components can accumulate photon-generated charges under light irradiation, and the charges can be read out for data processing and permanent storage. However, these cannot be easily realized from the optoelectronics made of a simple and single component of 2D semiconductor.

Recently, there are reports for design and fabrication of different optoelectronic memory devices based on multi-components of 2D semiconductor materials which have their potentials in neuromorphic visual systems. For example, the optoelectronic memory devices were reported to use MoS_2/h-BN/$CuInP_2S_6$/Cr/Au[29], MoS_2/h-BN/graphene floating-gated structure[25,26,30] and MoS_2/h-BN/gold nanoparticles (AuNPs) heterostructures.[13] There are other studies to exploit the structural defects of multi-component 2D materials which can produce charge trapping and releasing induced by light and electricity,[27,31] e.g., WSe_2/hBN design by adjusting electrons movement between the mid-gap defect states of BN and WSe_2,[32] and 2D materials hybridized with quantum dots[33]. These new 2D semiconductor designs can overcome the difficulties in controlling optoelectronic and memory properties. However, because of their complex structures and lack of large-scale preparation methods, they still have difficulties in high-density device integration and miniaturization of neuromorphic visual systems.

In this research, we solve these critical issues by designing and fabricating monolayer hydrophilic MoS_2 film through covalently introducing hydroxyl groups during its growth process. These hydroxyl groups exhibit a strong capability of charge trapping, which allows fabrication of optical memory transistors using a single component of monolayer hydrophilic MoS_2. Atomically thin neuromorphic vision systems are further manufactured from the arrays of optical memory transistors based on hydrophilic MoS_2 monolayer, with excellent capabilities of image sensing, image memorization, and color discrimination. The covalent bonding of these hydroxyl groups with monolayers of MoS_2 causes strong charge trapping, which makes the trapping and release of electrons can be controlled by laser and electric operations to realize stable image memory functions.

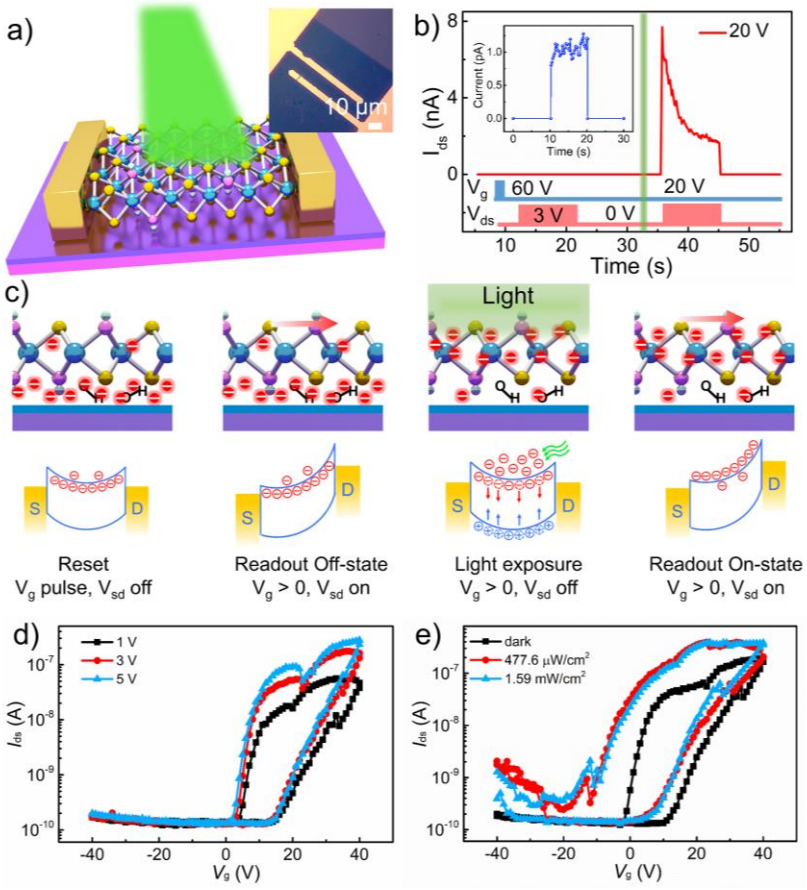

Fig. 2 MoS_2 optical memory transistor. (a) Schematic of the fabricated optical memory transistor based on MoS_2 under 550 nm laser. Inset: an optical image of the MoS_2 device. (b) Operating sequence and readout current of the MoS_2 optical memory transistor at 20 V gate voltage. A gate pulse (V_g = 60 V, 2 s) and a source-drain readout bias (V_{ds} = 3 V, 10 s) were applied for the reset and readout operations, respectively. The green vertical column indicates the period when the device was illuminated with a 550 nm laser with a power of 1.04 mW/cm^2. The inset represents an enlarged view of the readout current of Off-state. (c) Schematic of operational mechanism and energy band diagram of the MoS_2 optical memory transistor for the basic operations, depicting the initial state (reset operation), light exposure, and readout for Off- and On-states. (d) I_{ds}–V_g curves of the memory device under different V_{ds}. (e) I_{ds}–V_g curves of the memory device under a different light intensity of 550 nm laser at V_{ds}=3 V

Results and discussion

MoS_2 has been grown using various methods in literature.[34-40] In this work, we propose an alternative method to epitaxially grow monolayer of MoS_2 controlled using KOH. During this growth process, the hydroxyl groups in KOH solution will replace part of the S atoms in MoS_2, making the surface of MoS_2 with several hydroxyl groups. (see Fig. 1a) Since the hydroxyl groups have the ability to form hydrogen bonds with water, the hydrophilicity of the MoS_2 is increased. Fig. S1 schematically illustrates the precursor solution and spin-coating process used to synthesize the large-size monolayer of MoS_2 film. Details of procedures are provided in the Experimental Section. Contact angle, X-ray photoelectron spectroscopy (XPS), Raman spectroscopy, photoluminescence (PL) spectroscopy, atomic force microscope (AFM) and transmission electron microscope (TEM) are used to characterize the monolayer of MoS_2. Fig. 1a and Fig. 1b compare the hydrophilic and hydrophobic MoS_2 with their contact angles of 21° and 103°, respectively. The insets of Fig. 1a and Fig. 1b show the optical images of hydrophilic and hydrophobic MoS_2 on mica substrates, respectively. It clearly shows that the introduction of hydroxyl groups leads to the enhanced hydrophilicity of MoS_2.

To prove that the formation of hydrophilic MoS_2 is due to the covalently bonded hydroxyl groups on its surface, we perform XPS characterizations on both the surfaces of hydrophilic MoS_2 and the untreated MoS_2. Both MoS_2 samples are transferred from the mica substrates to p-type silicon substrates using a polymethyl methacrylate (PMMA) assisted transfer approach. Fig. 1c shows the XPS spectra of Mo 3d peaks for both hydrophilic MoS_2 and untreated MoS_2. It can be seen that binding energies of Mo $3d_{5/2}$ and $3d_{3/2}$ of hydrophilic MoS_2 are shifted about 0.4 eV than those of the untreated MoS_2, indicating that the chemical environment of Mo has changed in hydrophilic MoS_2. Furthermore, the Mo 3d spectrums are fitted to the doublet peaks of hydrophilic MoS_2 (at 229.6 and 232.7 eV) and untreated MoS_2 (at 230 and 233.1 eV) with ≈3.1 eV spin–

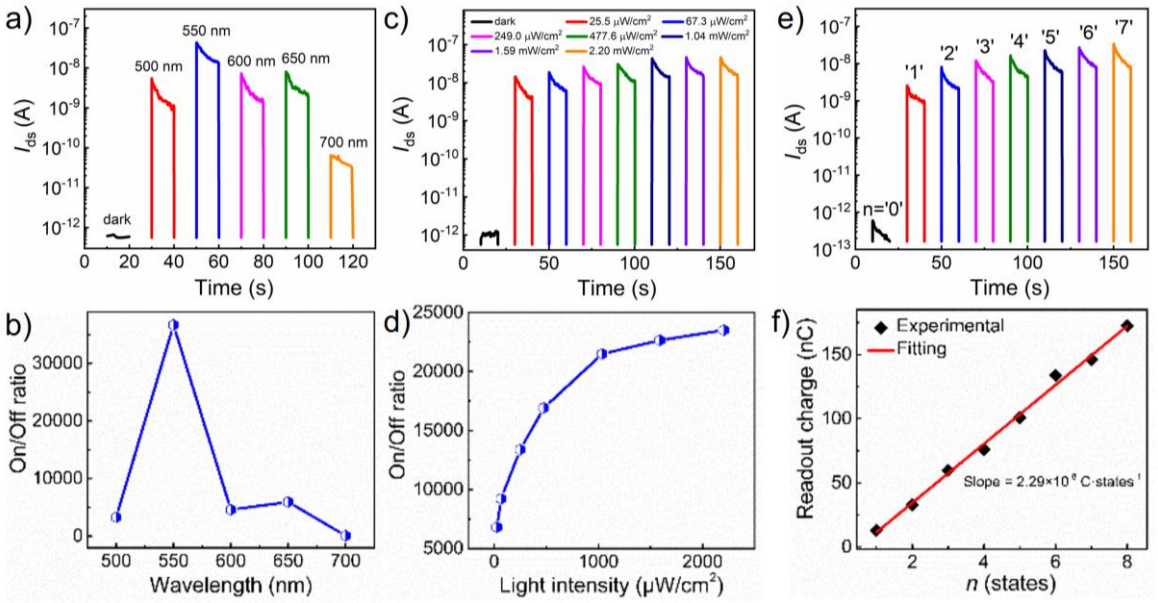

Fig. 3 Light-tunable characteristics of MoS_2 optical memory transistor. (a) The readout current as a function of light wavelength. The plots were separated with an interval of 10 s, regardless of the time that was measured initially. The light exposure time was 5 s, and the readout bias was applied after a 3 s waiting time. (b) The On/Off readout charge ratio as a function of light wavelength. (c) The readout current as a function of light intensity. The plots were separated with an interval of 10 s, regardless of the time that was measured initially. The light exposure time was 5 s, and the readout bias was applied after a 3 s waiting time. (d) The On/Off readout charge ratio as a function of light intensity. (e) Readout current as a function of the number of applied laser pulses, leading to eight different optical. (f) The On/Off readout charge ratio as a function of the number of applied laser pulses.

orbit splitting, corresponding to Mo^{4+} peaks of Mo-S bonds.[34] The small doublet peaks of hydrophilic MoS_2 (at 232.8 and 235.9 eV) and untreated MoS_2 (at 233.1 and 236.2 eV) provides evidences of the existence of low amounts of Mo^{6+}. Note that the peak at 227.3 eV corresponds to the binding energy of S 2s electrons. Different from untreated MoS_2, there are additional doublet peaks at 229.9 and 233 eV in Mo 3d spectrum of hydrophilic MoS_2, corresponding to Mo^{4+} peaks of Mo-O bonds.[41, 42] Additionally, to prove the existence form of oxygen atoms in hydrophilic MoS_2, the XPS spectra of O 1s peaks for both hydrophilic MoS_2 and untreated MoS_2 on p-type silicon substrates were analyzed. (Fig. 1d) For the hydrophilic MoS_2, O 1s components at 532.8, 532.2 and 531.7 eV are linked to those of the natural oxide layer,[43] adsorbed oxygen on silicon substrates[44] and hydroxyl groups,[45] indicating the presence of hydroxyl groups in the hydrophilic MoS_2 sample. Whereas for that of the untreated MoS_2, there is only two major peaks at 532.9 and 532.3 eV, which is linked with that of natural oxide layer, adsorbed oxygen on silicon substrates. Meanwhile, Fig. S2a shows that S $2p_{1/2}$ and S $2p_{3/2}$ peaks of hydrophilic MoS_2 are located at 163.6 and 162.4 eV, implying the formation of MoS_2. Fig. S2b shows the corresponding full XPS spectra of hydrophilic MoS_2 on p-type silicon substrate. Fig. S3a displays the binding energies of the S $2p_{1/2}$ and S $2p_{3/2}$ peaks as well as the full XPS spectra of the untreated MoS_2. XPS analysis proves that for the hydrophilic MoS_2 we synthesized, the hydroxyl groups replace part of the sulfur atoms in MoS_2 and are covalently connected to the molybdenum atom.

Furthermore, Raman and PL measurements of the hydrophilic MoS_2 are carried out with a 532 nm laser at roomtemperature. The inset of Figure 1f is the optical image of MoS_2 on SiO_2. Fig. 1e shows Raman spectra of the hydrophilic MoS_2 and untreated MoS_2 samples transfered on SiO_2 substrates. The E^1_{2g} mode and the A_{1g} mode represent the in-plane vibration and out-of-plane vibration, respectively.[37] Comparing to pristine MoS_2, the positions of E^1_{2g} and A_{1g} of hydrophilic MoS_2 undergo a red shift, indicating the evolution of lattice dynamics. In additon, the full widths at half-maximum (fwhm) of the two peaks have increased and A_{1g} peak has stronger intensity than E^1_{2g} peak in hydrophilic MoS_2. These phenomena are due to the substitution of the S atoms in MoS_2 by the hydroxyl groups, which leads to the enhancement of the crystal disorder and weakening of out-of-plane vibration of S atoms.[46] The frequency differences between the E^1_{2g} and A_{1g} peak of both samples are less than 20 cm^{-1}, demonstrating the formation of monolayer MoS_2.[39] Raman mapping image of the E^1_{2g} peak is shown in Fig. S4, which confirms that the monolayer MoS_2 exhibits a good uniformity. Fig. 1f displays a typical PL spectrum of monolayer MoS_2 grown on mica and an intense PL peak is observed at 1.84 eV, which is another evidence of formation of MoS_2 monolayer.[4] Fig. 1g is an AFM topography image of MoS_2 transfered on SiO_2/Si substrate. From the height profile, the thickness of the MoS_2 layer is ~1 nm, confirming the formation of the monolayer MoS_2.[37,38]

Crystalline structure and crystal quality of the MoS_2 monolayer are observed directly using selected area electron diffraction (SAED) and high-resolution TEM (HRTEM). Fig. S5a shows that the MoS_2 has hexagonally symmetrical SAED

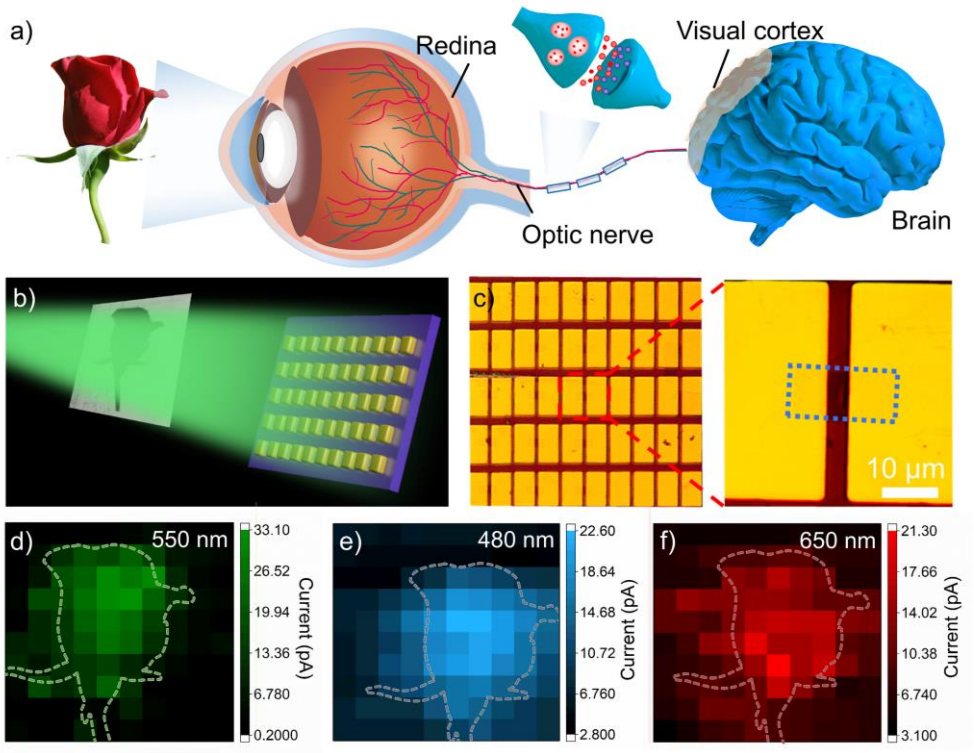

Fig. 4 Neuromorphic vision sensors with color resolution. (a) Schematic diagram of natural visual systems and related afferent nerve system. (b) The artificial neuromorphic vision systems based on the MoS_2 optical memory transistor. (c) Optical images of these MoS_2 artificial neuromorphic vision systems. An illustration of the image memory after 1 min (d) under 550 nm, (e) 480 nm, and (f) 650 nm laser with a power of 1.04 mW/cm^2 at 100 mV.

patterns of single crystals.[47] Furthermore, HRTEM analysis in Fig. S5b shows that the lattice distance is ~0.27 nm, which is in a good agreement with that of (100) plane (marked as red line). This clearly suggests the high-crystalline quality of the prepared MoS_2.

Optical memory transistors are fabricated from the single component of as-prepared hydrophilic MoS_2 monolayer and a trap control switching mechanism of the hydrophilic MoS_2 optical memory devices is proposed based on the nonvolatile characteristics. [48,49] Fig. 2a shows a schematic illustration of the MoS_2 optical memory device based on a field effect transistor (FET) structure with electrodes of Au. The inset of Fig. 2a is an optical image of the memory device. In addition, the output curves of this hydrophilic MoS_2 FET is shown in Fig. S6, demonstrating the Schottky contact between the MoS_2 and Au electrodes. Then a potential well is formed between Au electrodes and MoS_2 monolayer with a bending energy band. Fig. 2b displays one operation cycle based on this MoS_2 device, demonstrating a good memory function. Firstly, a large positive gate pulse (60 V) is applied as Reset operation to make plentiful of electrons from the conduction band fill the trap level, which results the conduction band is decreased and below the trap level. In the n-type MoS_2 semiconductor, electron carriers are accumulated and trapped due to the existence of hydroxyl groups. When a lower gate voltage (Initial voltage) is applied, the trapped electrons cannot easily be released, thus resulting in the decrease of the electron concentration in the conduction band. Then a source-drain voltage of 3V (10 s) is applied to read the Off-state current. The inset in Fig. 2b represents an enlarged view of the readout current of Off-state. A fairly low Off-state current of ~1 pA can be obtained and the readout charge (Q_{ph}) integrated for 10 s is found to be about 1 pC. To release the trapped electrons, a laser pulse (5 s) is applied to the MoS_2 optical memory devices, which leads to a considerable number of electron-hole pairs generated. These photon-generated electrons come from both the valence band and trap level, thus resulting in the vast electrons in the conduction band. A period of time after the illumination, a source-drain voltage of 3 V (10 s) is applied again to read the On-state current. As a result, a large On-state readout charge of about 27.1 nC and a On/Off ratio of ~2.7×10^4 can be achieved. The current of On-state has a tendency to decrease to its original current because of the electron-hole recombination, which means that long-term information storage cannot be achieved. The corresponding schematic of operational mechanism and energy band diagram of the hydrophilic MoS_2 optical memory devices is schematically shown in Fig. 2c.

To further prove the effectiveness of these functional hydroxyl groups and exclude the effect of defect states in CVD-grown MoS_2 on properties, a device of the same structure based on MoS_2 without hydroxyl groups is fabricated and tested (Fig. S7a). A same operation cycle is conducted on the MoS_2 device without hydroxyl groups, and results show that there is no optical memory (Fig. S7b). Therefore, we can confirm that this MoS_2 optical memory operation mechanism is truly based on strong charge trapping states caused by these hydroxyl groups

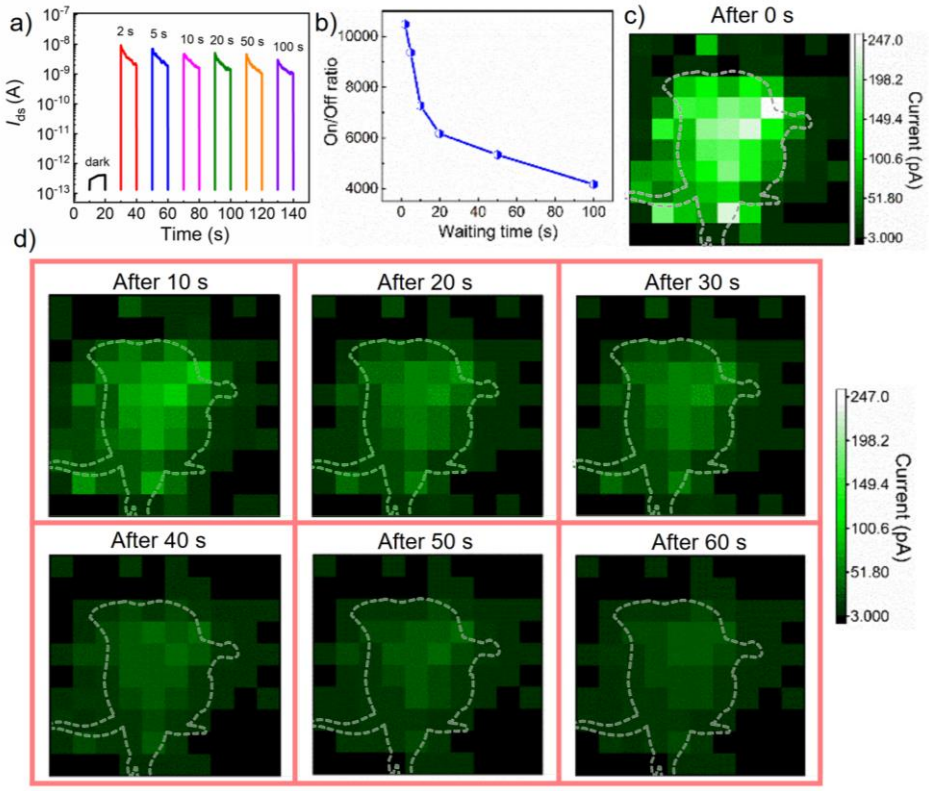

Fig. 5 Neuromorphic vision sensors for different waiting times. (a) Readout current as a function of waiting time. (b) The On/Off readout charge ratio for different waiting times. (c) An illustration of the image after illuminated 10 s under 550 nm laser with a power of 1.04 mW/cm^2 at 100 mV. (d) An illustration of the image memory under 550 nm laser with a power of 1.04 mW/cm^2 at 100 mV. The light exposure time was 10 s, and the readout bias was applied after waiting time of 10 s, 20 s, 30 s, 40 s, 50 s, and 60 s respectively.

covalently bonded with MoS_2. The results can well explain the performance of the device under different conditions and prove its good wavelength and light intensity resolutions, thus providing advantages for the applications in the neuromorphic visual systems.

The electrical control of MoS_2 memory devices is further invetigated in order to show the storage control capabilities of our devices. Fig. 2d and Fig. 2e show the transfer curves under different source-drain voltages V_{ds} and different light intensities of 550 nm laser, respectively. Memory window (ΔV), defined as the difference between two threshold voltages when V_g is swept from positive to negative and then back to positive, indicates the storage capacity of devices.[50] The ΔV values of transfer curves under different light intensities (P_i) are broadened to 29.6 V with a light intensity of 1.59 mW/cm^2, which exhibits that the electrical hysteresis can be enhanced by applying higher values of P_i. Furthermore, the hysteretic behaviour and ΔV of hydrophilic MoS_2 FETs is related to the density of trapped charges (N_{trap}). It can be assumed that the difference in the threshold voltage of hydrophilic MoS_2 FET is due to the N_{trap} on one side of a capacitor.[10, 51] The N_{trap} can be estimated by the following formula:

$$N_{trap} \approx \frac{C_{ox} \times \Delta V_{th}}{q}$$

where C_{ox} is the capacitance/area of the gate dielectric, ΔV_{th} is the memory window and q is the electronic charge. Using this method, the density of trapped charges of hydrophilic MoS_2 FET under different V_{ds} and light intensity are shown in Fig. S8a and Fig. S8b, respectively. It is worth noting that there is a kink in the transfer curve. When the gate voltage becomes more and more positive and reaches a certain value, the initially trapped electrons in hydrophilic MoS_2 are released, reducing the electron concentration in MoS_2. By comparing the transfer curves of the devices of MoS_2 with hydroxyl groups (red) and without hydroxyl groups (blue) shown in Fig. S9a, we can conclude that the introduction of hydroxyl groups enhances the memory property of MoS_2 devices. Additionally, Fig. S9b are the corresponding I_g vs V_g curves with different positive V_g ranges of hydrophilic MoS_2 FET, exhibiting the variation of leakage current.

We have further done five separate operation cycles based on this MoS_2 memory device under different initial voltages, and the results are shown in Fig. S10. The readout charges for both the Off-state and On-state are increased as the initial voltage is increased, which is due to the enhancement of carrier densities in the channel at a higher gate voltage. The On/Off ratio of the readout charge reaches its highest value at around 1.7×10^4 when the device is operated with a gate voltage of 20 V (Fig. S11). The On/Off ratio is less than 2 without applying reset operation (Fig. S12), demonstrating the effective reset function for this MoS_2 optical memory devices.

Furthermore, light-dependent performances of the as-fabricated MoS_2 optical memory transistors are investigated at different laser wavelengths and light intensities. Fig. 3a shows the readout currents with different wavelengths from 500 nm to 700 nm under a light intensity of ~2.2 mW/cm^2, suggesting that this MoS_2 optical memory transistor has the ability of wavelength identification because the introduction of hydroxyl groups on the surface, in principle, does not change the intrinsic properties of MoS_2. The corresponding Off-state currents under different light wavelengths are shown in Fig.S13a. The device has the best sensitivity to 550 nm light with a maximum readout charge of 218 nC (Fig. S13b). A lot of electron-hole pairs are generated at this condition, resulting in that the electrons dominantly exist in the conduction band. The corresponding maximum On/Off readout charge ratio is 3.7×10^4 (Fig. 3b).

Fig. 3c shows the readout currents at different light intensities of 550 nm laser. In addition, Fig. S13c exhibits the Off-state currents under different light intensities. The Off-state current of each test is basically unchanged, and the On-state current is enhanced with the increase of light intensity, thereby increasing the switching ratio. Fig. S13d shows the readout charges extracted from Fig. 3c as a function of light intensity. The readout charge shows a power-law dependence as a function of the light intensity with an exponent of 0.27 ($Q_{ph} \approx P_i^{0.27}$), which indicates that the readout charge is dramatically enhanced by increasing the light intensity. The higher the light intensity, the more electrons in the conduction band per unit time are extracted from the valence band and defect energy level, which leads to more readout charges. Moreover, this non-integer exponent of 0.27 can be associated with the strong trap states, which are due to the hydroxyl groups covalently bonded with MoS_2. [52,53] Fig. 3d shows the On/Off readout charge ratios obtained under different light intensities. The higher the light intensity, the greater the switching ratio, indicating a high sensitivity of our device to light intensity.

The multi-bit storage of our MoS_2 optical memory transistor is further investigated. Fig. 3e shows the obtained readout currents as a function of the number of applied laser pulses. The readout current gradually increases with the increase of applied laser pulses at the same level of Off-state current (Fig. S13e). Fig. 3f shows that the collected readout charge in the On-state recorded is ~10 s. The line of best fit (red) indicates that the readout charge has a linear relationship with the number of laser pulses and increases by 20 nC after each laser pulse, which also demonstrates that the multi-bit storage of this MoS_2 optical memory transistor is reliable for multiple tests. The On/Off readout charge ratio is enhanced from ~4.6×10^3 to ~5.1×10^4 as shown in Fig. S13f. These findings show that multi-bit storage can be controlled by the number of applied laser pulses, suggesting the potential for application in storing complex information.

Fig. 4a and Fig. 4b show comparisons of the human neuromorphic visual system and biomimetic vision system. In the neuromorphic visual system of human beings, optical signals perceived by the light-receptive cells on the retina are transferred to the visual cortex of the brain to process and analyze via their connection optic nerves composed of synapses (Fig. 4a). This natural system has inspired the research and development of artificial neuromorphic vision systems. [54,55] In this study, the atomically thin biomimetic vision system is, for the first time, realized by using the arrays of hydrophilic MoS_2 monolayer optical memory transistors (Fig. 4b). Fig. 4c shows the optical images of the device arrays. Using an optical mask of "rose", the pixels are illuminated by a light pulse of 10 s simultaneously and the channel current of each pixel is measured after a waiting time of 1 min sequentially. To demonstrate the color resolution of MoS_2 neuromorphic visual sensors, light pulses of 550 nm, 480 nm, and 650 nm are applied on the array, respectively. After the removal of light stimuli for 1 min, three "roses" images with different colors are recorded and the results are shown in Fig. 4d, Fig. 4e, and Fig. 4f. Compared to the area sheltered by an optical mask, the other parts which have been illuminated by the light with different wavelengths show higher photocurrents of about dozens of pA, resulting in the formation of flower "rose" image. Although each pixel does not show the exactly same current, the flower "rose" can still be distinguished from different colors due to the differences among photo memory currents received by lights with three wavelengths under same light intensity, indicative of reliable image memorization and color resolution capabilities of the MoS_2 neuromorphic visual sensors. Furthermore, in order to prove the uniformity of our array, the image diagrams of the Off-state current of the device and after 10 s of illumination at 100 mV without mask are shown in Fig. S14a and Fig. S14b, respectively.

The atomically thin biomimetic vision system is also capable to show time-dependent properties including light exposure duration and waiting time after light illumination, which will be of great significance for emulating the basic learning and memory functions of the human brain. Fig. S15a shows the readout currents of light exposure times from 0.5 to 100 s and the corresponding Off-state currents are displayed in Fig. S15b. Fig. S15c shows the readout charge data extracted from Fig. S15a, which is positively dependent on the light exposure time. The introduction of hydroxyl groups causes a large number of trap states in the device, which signficantly hinders the recombination of electrons and holes. Therefore, with the increase of light exposure duration, more electrons are accumulated in the conduction band, thus gradually increasing the current. The corresponding On/Off readout charge ratio is also increased as the light exposure duration is extended (Figure S15d).

The charge storage lifetime is important for image sensing and memory devices. The readout currents as a function of the waiting time are measured and the results are shown in Fig. 5a. The waiting time is defined as the time between the end of the illumination and the application of the read voltage (with the light exposure time is fixed at 10 s). The On-state current gradually decreases with the increase of waiting time under basically unchanged Off-state currents. (Fig. S16a) The fitting result of the readout charge within 10 s satisfies an exponential relationship ($Q_{ph} = 4.62\cdot10^{-8}t^{-0.23}$), from which the time drop to 20% is about 100 s, suggesting the non-volatile storage performance of the MoS_2 optical memory device (Fig. S16b). Moreover, the extremely low Off-state charge of 3.65 pC is due

to the application of a 60 V gate voltage, so that the On-state charge is decreased with time, and eventually will not reach the Off-state charge. Fig. 5b shows that the On/Off readout charge ratio is decreased with the waiting time before readout adding from 2 s to 100 s.

The corresponding image evolution of MoS_2 neuromorphic visual sensors at different waiting times has further been studied. Fig. 5c shows one image of the sensor after illuminated for 10 s under a 550 nm laser with a power of 1.04 mW/cm^2 at 100 mV. Fig. 5d show results of the image memory when the readout bias is applied after waiting times of 10 s, 20 s, 30 s, 40 s, 50 s and 60 s, respectively, exhibiting the condition of image evolution and image memorization of the MoS_2 neuromorphic visual sensors. These results are of great significance for the practical application such as cameras and fax machines.

Conclusions

In this work, we have prepared monolayer hydrophilic MoS_2 films covalently bonded with hydroxyl groups with strong charge trapping capability, which allows the realization of filter-free optical memory transistors. These optical memory transistors based on a single component of monolayer hydrophilic MoS_2 can capture or release electrons through the application of light and adjustment of the gate voltage, thus resulting in a good nonvolatile optoelectronic memory performance. The storage charge can be effectively modulated by the light intensity, wavelength, illumination time, retention time, and numbers of light pulses. Multi-bit storage and more than 10^4 switching ratio can be realized. Furthermore, to demonstrate image sensing, image memorization, and color discrimination, we fabricate neuromorphic visual systems consisted of arrays of hydrophilic MoS_2 monolayer optical memory transistors. Our work demonstrates that monolayer hydrophilic MoS_2 film is a promising candidate in the field of artificial visual systems and could open up new opportunities for practical applications of miniaturization of advanced neuromorphic visual systems.

Conflicts of interest

There are no conflicts to declare.

Acknowledgements

This work is supported by National Basic Research Program of China (2019YFB1310200), Foundation for Innovative Research Groups of the National Natural Science Foundation of China (no. 51521003), National Postdoctoral Science Foundation of China (no.2017M621254, 2018T110280), Heilongjiang Provincial Postdoctoral Science Foundation (no. LBH-TZ1708), Self-Planned Task of State Key Laboratory of Robotics and System (HIT) (no. SKLRS201607B), Engineering Physics and Science Research Council of UK (EPSRC EP/P018998/1) and Newton Mobility Grant (IE161019) through Royal Society and Natural Science Foundation of China.

References

1. Q. H. Wang, K. Kalantar-Zadeh, A. Kis, J. N. Coleman and M. S. Strano, *Nat. Nanotechnol.*, 2012, **7**, 699-712.
2. O. Lopez-Sanchez, D. Lembke, M. Kayci, A. Radenovic and A. Kis, *Nat. Nanotechnol.*, 2013, **8**, 497-501.
3. F. H. Koppens, T. Mueller, P. Avouris, A. C. Ferrari, M. S. Vitiello and M. Polini, *Nat. Nanotechnol.*, 2014, **9**, 780-793.
4. K. F. Mak, C. Lee, J. Hone, J. Shan and T. F. Heinz, *Phys. Rev. Lett.*, 2010, **105**, 136805.
5. H. Shang, H. Chen, M. Dai, Y. Hu, F. Gao, H. Yang, B. Xu, S. Zhang, B. Tan, X. Zhang and P. Hu, *Nanoscale Horizons*, 2020, **5**, 564-572.
6. M. Dai, Z. Wang, F. Wang, Y. Qiu, J. Zhang, C. Y. Xu, T. Zhai, W. Cao, Y. Fu, D. Jia, Y. Zhou and P. A. Hu, *Nano Lett.*, 2019, **19**, 5410-5416.
7. W. Feng, W. Zheng, W. Cao and P. Hu, *Adv. Mater.*, 2014, **26**, 6587-6593.
8. M. Dai, H. Chen, R. Feng, W. Feng, Y. Hu, H. Yang, G. Liu, X. Chen, J. Zhang, C. Y. Xu and P. Hu, *ACS Nano*, 2018, **12**, 8739-8747.
9. W. Li, M. Dai, Y. Hu, H. Chen, X. Zhu, Q. Yang and P. Hu, *ACS Appl. Mater. Interfaces*, 2019, **11**, 47098-47105.
10. S. Zhang, Y. Qiu, H. Yang, D. Wang, Y. Hu, X. Lu, Z. Li and P. Hu, *Journal of Materials Chemistry C*, 2020, DOI: 10.1039/d0tc00331j.
11. B. Radisavljevic, A. Radenovic, J. Brivio, V. Giacometti and A. Kis, *Nat. Nanotechnol.*, 2011, **6**, 147-150.
12. M. Dai, W. Zheng, X. Zhang, S. Wang, J. Lin, K. Li, Y. Hu, E. Sun, J. Zhang, Y. Qiu, Y. Fu, W. Cao and P. Hu, *Nano Lett.*, 2020, **20**, 201-207.
13. D. Lee, E. Hwang, Y. Lee, Y. Choi, J. S. Kim, S. Lee and J. H. Cho, *Adv. Mater.*, 2016, **28**, 9196-9202.
14. S. Lei, F. Wen, B. Li, Q. Wang, Y. Huang, Y. Gong, Y. He, P. Dong, J. Bellah, A. George, L. Ge, J. Lou, N. J. Halas, R. Vajtai and P. M. Ajayan, *Nano Lett.*, 2015, **15**, 259-265.
15. A. Splendiani, L. Sun, Y. Zhang, T. Li, J. Kim, C. Y. Chim, G. Galli and F. Wang, *Nano Lett.*, 2010, **10**, 1271-1275.
16. H. C. Ko, M. P. Stoykovich, J. Song, V. Malyarchuk, W. M. Choi, C. J. Yu, J. B. Geddes, 3rd, J. Xiao, S. Wang, Y. Huang and J. A. Rogers, *Nature*, 2008, **454**, 748-753.
17. S. Ambrogio, P. Narayanan, H. Tsai, R. M. Shelby, I. Boybat, C. di Nolfo, S. Sidler, M. Giordano, M. Bodini, N. C. P. Farinha, B. Killeen, C. Cheng, Y. Jaoudi and G. W. Burr, *Nature*, 2018, **558**, 60-67.
18. Y. M. Song, Y. Xie, V. Malyarchuk, J. Xiao, I. Jung, K. J. Choi, Z. Liu, H. Park, C. Lu, R. H. Kim, R. Li, K. B. Crozier, Y. Huang and J. A. Rogers, *Nature*, 2013, **497**, 95-99.
19. G. J. Lee, C. Choi, D. H. Kim and Y. M. Song, *Adv. Funct. Mater.*, 2017, **28**.
20. S. Yu, B. Gao, Z. Fang, H. Yu, J. Kang and H. S. Wong, *Adv. Mater.*, 2013, **25**, 1774-1779.
21. F. Zhou, Z. Zhou, J. Chen, T. H. Choy, J. Wang, N. Zhang, Z. Lin, S. Yu, J. Kang, H. P. Wong and Y. Chai, *Nat. Nanotechnol.*, 2019, **14**, 776-782.
22. H. Wang, H. Liu, Q. Zhao, Z. Ni, Y. Zou, J. Yang, L. Wang, Y. Sun, Y. Guo, W. Hu and Y. Liu, *Adv. Mater.*, 2017, **29**.
23. K.-H. Jeong, J. Kim and L. P. Lee, *Science*, 2006, **312**, 557.
24. R. Chen, A. Canales and P. Anikeeva, *Nat. Rev. Mater.*, 2017, **2**.
25. W. Huang, L. Yin, F. Wang, R. Cheng, Z. Wang, M. G. Sendeku, J. Wang, N. Li, Y. Yao, X. Yang, C. Shan, T. Yang and J. He, *Adv. Funct. Mater.*, 2019, **29**.
26. S. H. Kim, S.-G. Yi, M. U. Park, C. Lee, M. Kim and K.-H. Yoo, *ACS Appl. Mater. Interfaces*, 2019, **11**, 25306-25312.
27. H. Liu, M. Cui, C. Dang, W. Wen, X. Wang and L. Xie, *ACS Appl. Mater. Interfaces*, 2019, **11**, 34424-34429.
28. F. Zhou, J. Chen, X. Tao, X. Wang and Y. Chai, *Research (Wash D C)*,

2019, **2019**, 9490413.
29. W. Huang, F. Wang, L. Yin, R. Cheng, Z. Wang, M. G. Sendeku, J. Wang, N. Li, Y. Yao and J. He, *Adv. Mater.*, 2020, **32**, e1908040.
30. M. D. Tran, H. Kim, J. S. Kim, M. H. Doan, T. K. Chau, Q. A. Vu, J. H. Kim and Y. H. Lee, *Adv. Mater.*, 2019, **31**, e1807075.
31. J. Lee, S. Pak, Y. W. Lee, Y. Cho, J. Hong, P. Giraud, H. S. Shin, S. M. Morris, J. I. Sohn, S. Cha and J. M. Kim, *Nat. Commun.*, 2017, **8**, 14734.
32. D. Xiang, T. Liu, J. Xu, J. Y. Tan, Z. Hu, B. Lei, Y. Zheng, J. Wu, A. H. C. Neto, L. Liu and W. Chen, *Nat. Commun.*, 2018, **9**.
33. Y. Zhai, X. Yang, F. Wang, Z. Li, G. Ding, Z. Qiu, Y. Wang, Y. Zhou and S. T. Han, *Adv. Mater.*, 2018, **30**, e1803563.
34. J. Zhu, H. Xu, G. Zou, W. Zhang, R. Chai, J. Choi, J. Wu, H. Liu, G. Shen and H. Fan, *J. Am. Chem. Soc.*, 2019, **141**, 5392-5401.
35. A. Aljarb, Z. Cao, H. L. Tang, J. K. Huang, M. Li, W. Hu, L. Cavallo and L. J. Li, *ACS Nano*, 2017, **11**, 9215-9222.
36. D. Fu, X. Zhao, Y. Y. Zhang, L. Li, H. Xu, A. R. Jang, S. I. Yoon, P. Song, S. M. Poh, T. Ren, Z. Ding, W. Fu, T. J. Shin, H. S. Shin, S. T. Pantelides, W. Zhou and K. P. Loh, *J. Am. Chem. Soc.*, 2017, **139**, 9392-9400.
37. Q. Ji, Y. Zhang, T. Gao, Y. Zhang, D. Ma, M. Liu, Y. Chen, X. Qiao, P. H. Tan, M. Kan, J. Feng, Q. Sun and Z. Liu, *Nano Lett.*, 2013, **13**, 3870-3877.
38. J. Lee, S. Pak, P. Giraud, Y. W. Lee, Y. Cho, J. Hong, A. R. Jang, H. S. Chung, W. K. Hong, H. Y. Jeong, H. S. Shin, L. G. Occhipinti, S. M. Morris, S. Cha, J. I. Sohn and J. M. Kim, *Adv. Mater.*, 2017, **29**.
39. K. Suenaga, H. G. Ji, Y. C. Lin, T. Vincent, M. Maruyama, A. S. Aji, Y. Shiratsuchi, D. Ding, K. Kawahara, S. Okada, V. Panchal, O. Kazakova, H. Hibino, K. Suenaga and H. Ago, *ACS Nano*, 2018, **12**, 10032-10044.
40. S. Wang, Y. Rong, Y. Fan, M. Pacios, H. Bhaskaran, K. He and J. H. Warner, *Chem. Mater.*, 2014, **26**, 6371-6379.
41. J. Tang, Z. Wei, Q. Wang, Y. Wang, B. Han, X. Li, B. Huang, M. Liao, J. Liu, N. Li, Y. Zhao, C. Shen, Y. Guo, X. Bai, P. Gao, W. Yang, L. Chen, K. Wu, R. Yang, D. Shi and G. Zhang, *Small*, 2020, DOI: 10.1002/smll.202004276, e2004276.
42. K. Akiyoshi, T. Kameyama, T. Yamamoto, S. Kuwabata, T. Tatsuma and T. Torimoto, *RSC Adv.*, 2020, **10**, 28516-28522.
43. S. Salimian and M. Delfino, *J. Appl. Phys.*, 1991, **70**, 3970-3972.
44. V. D. Borman, E. P. Gusev, Y. Y. Lebedinski and V. I. Troyan, *Physical Review B*, 1994, **49**, 5415-5423.
45. B. Brox and I. Olefjord, *Surf. Interface Anal.*, 1988, **13**, 3-6.
46. N. Kang, H. P. Paudel, M. N. Leuenberger, L. Tetard and S. I. Khondaker, *The Journal of Physical Chemistry C*, 2014, **118**, 21258-21263.
47. H. Liu, F. Gao, Y. Hu, J. Zhang, L. Wang, W. Feng, J. Hou and P. Hu, *2D Materials*, 2019, **6**.
48. L. Wang, L. Chen, S. L. Wong, X. Huang, W. Liao, C. Zhu, Y. F. Lim, D. Li, X. Liu, D. Chi and K. W. Ang, *Adv. Electron. Mater.*, 2019, **5**.
49. L. Wang, W. Liao, S. L. Wong, Z. G. Yu, S. Li, Y. F. Lim, X. Feng, W. C. Tan, X. Huang, L. Chen, L. Liu, J. Chen, X. Gong, C. Zhu, X. Liu, Y. W. Zhang, D. Chi and K. W. Ang, *Adv. Funct. Mater.*, 2019, **29**.
50. D. J. Late, B. Liu, H. S. S. R. Matte, V. P. Dravid and C. N. R. Rao, *ACS Nano*, 2012, **6**, 5635-5641.
51. M. McDowell, I. G. Hill, J. E. McDermott, S. L. Bernasek and J. Schwartz, *Appl. Phys. Lett.*, 2006, **88**, 073505.
52. W. Y. Kong, G. A. Wu, K. Y. Wang, T. F. Zhang, Y. F. Zou, D. D. Wang and L. B. Luo, *Adv. Mater.*, 2016, **28**, 10725-10731.
53. W. Feng, X. Wang, J. Zhang, L. Wang, W. Zheng, P. Hu, W. Cao and B. Yang, *J. Mater. Chem. C*, 2014, **2**, 3254-3259.
54. T. Ahmed, S. Kuriakose, E. L. H. Mayes, R. Ramanathan, V. Bansal, M. Bhaskaran, S. Sriram and S. Walia, *Small*, 2019, **15**, e1900966.
55. S. G. Kim, S. H. Kim, J. Park, G. S. Kim, J. H. Park, K. C. Saraswat, J. Kim and H. Y. Yu, *ACS Nano*, 2019, **13**, 10294-10300.